Ionics (2016) 22:209–218
DOI 10.1007/s11581-015-1541-9

ORIGINAL PAPER

Synthesis and electrochemical properties of $Li_{1.2}Mn_{0.54}Ni_{0.13}Co_{0.13}O_2$ cathode material for lithium-ion battery

ChenQiang Du[1] · Fei Zhang[1] · ChenXiang Ma[1] · JunWei Wu[2] · ZhiYuan Tang[1] · XinHe Zhang[3] · Deyang Qu[3,4]

Received: 16 June 2015 / Revised: 23 July 2015 / Accepted: 16 August 2015 / Published online: 2 September 2015

Abstract The layered $Li_{1.2}Mn_{0.54}Ni_{0.13}Co_{0.13}O_2$ lithium-rich manganese-based solid solution cathode material has been synthesized by a simple solid-state method. The as-prepared material has a typical layered structure with R-3m and C2/m space group. The synthesized $Li_{1.2}Mn_{0.54}Ni_{0.13}Co_{0.13}O_2$ has an irregular shape with the size range from 200 to 500 nm, and the primary particle of $Li_{1.2}Mn_{0.54}Ni_{0.13}Co_{0.13}O_2$ has regular sphere morphology with a diameter of 320 nm. Electrochemical performances also have been investigated. The results show that the cathode material $Li_{1.2}Mn_{0.54}Ni_{0.13}Co_{0.13}O_2$ prepared at 900 °C for 12 h has a good electrochemical performance, which can deliver a high initial discharge capacity of 233.5, 214.2, 199.3, and 168.1 mAh g^{-1} at 0.1, 0.2, 0.5, and 1 C, respectively. After 50 cycles, the capacity retains 178.0, 166.3, 162.1, and 155.9 mAh g^{-1} at 0.1, 0.2, 0.5, and 1 C, respectively. The results indicate that the simple method has a great potential in synthesizing manganese-based cathode materials for Li-ion batteries.

Keywords Lithium-ion battery · Lithium-rich metal oxides · $Li_{1.2}Mn_{0.54}Ni_{0.13}Co_{0.13}O_2$ · Solid-state method

✉ ChenQiang Du
dcqxinyang@126.com

✉ ZhiYuan Tang
1013207103@tju.edu.cn

[1] Department of Applied Chemistry, School of Chemical Engineering and Technology, Tianjin University, Tianjin 300072, China

[2] School of Materials Science and Engineering, Harbin Institute of Technology Shenzhen Graduate School, Shenzhen 518055, China

[3] McNair Technology Company, Limited, Dongguan City, Guangdong 523700, China

[4] Department of Chemistry, University of Massachusetts Boston, 100 Morrissey Blvd., Boston, MA 02125, USA

Introduction

Recently, lithium-ion batteries have been considered as the dominant power sources for large-scale applications, such as electric vehicles (EV) and hybrid electric vehicles (HEV) [1–3]. While conventional cathode materials, such as olivine $LiFePO_4$ [4], spinel $LiMn_2O_4$ [5], and layered $LiMO_2$ (M=Ni, Co, Mn, etc.) [6–8], cannot meet the increasing demands for high-energy and high-power batteries due to limited theoretical capacity. Searching for high-capacity and safe alternatives has become one of the most important subjects. The material system based on the layered-layered compositions of $xLi_2MnO_3 \cdot (1-x)LiMO_2$ (M=Ni, Mn, etc.) has recently attracted more and more attention due to low cost, environmental friendliness, and higher capacity [9–11]. Lithium-excess layered oxides $xLi_2MnO_3 \cdot (1-x)LiMO_2$ (M=Ni, Mn, etc.) are composed of the intergrowth of $LiMO_2$ (R3m) and Li_2MnO_3 (C2/m) phases and can deliver higher capacity (>250 mA h g^{-1}) with relatively high operating voltage (3.5 V versus Li/Li+on average). However, there are several disadvantages such as high first cycle irreversible capacity and inherently low rate capability, which limit its application. Thus, various strategies have been used to improve its electrochemical performances, most of which involves reducing particle size [12, 13] or coating with other materials [14–16] and doping with different elements [10, 17, 18]. Compared with doping and coating methods, reducing particle size is an effective way to improve the properties of as-prepared materials without degrading the intrinsic properties [19]. Meanwhile, synthesis method has significant effects on the morphology and particle size of materials [19, 20]. Solid-state approach is considered to be one of the simplest methods, which has been applied widely in the synthesis of electrode materials [21–24].

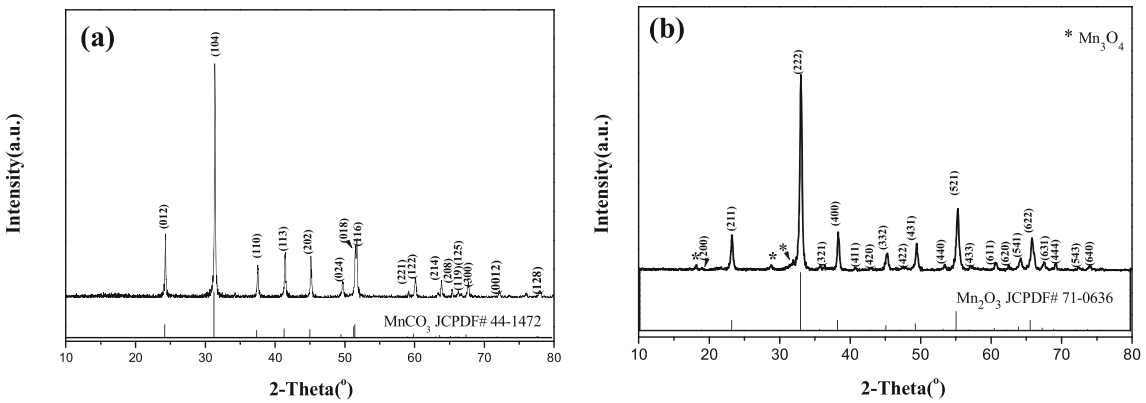

Fig. 1 XRD patterns of the $MnCO_3$ (**a**) and Mn_2O_3 (**b**) and cathode material $Li_{1.2}Mn_{0.54}Ni_{0.13}Co_{0.13}O_2$ synthesized at 900° C for different time

During conventional synthesis of Li_2MnO_3-$LiMO_2$, the raw materials usually have micrometer scale with irregular morphology and mixed by grinding or ball-milling methods. After high-temperature sintering process, the resultant products are usually composed of irregular nano- or microparticles due to undesirable particle growth, although the undesirable particle growth can be partly inhibited by adding growth inhibitors [25, 26]. However, morphology and size control of Li_2MnO_3-$LiMO_2$ nanostructures remain a great challenge. Herein, we present a simple and feasible synthesis of $Li_{1.2}Mn_{0.54}Ni_{0.13}Co_{0.13}O_2$ microspheres with nano-sized subunits by a precipitation method followed by

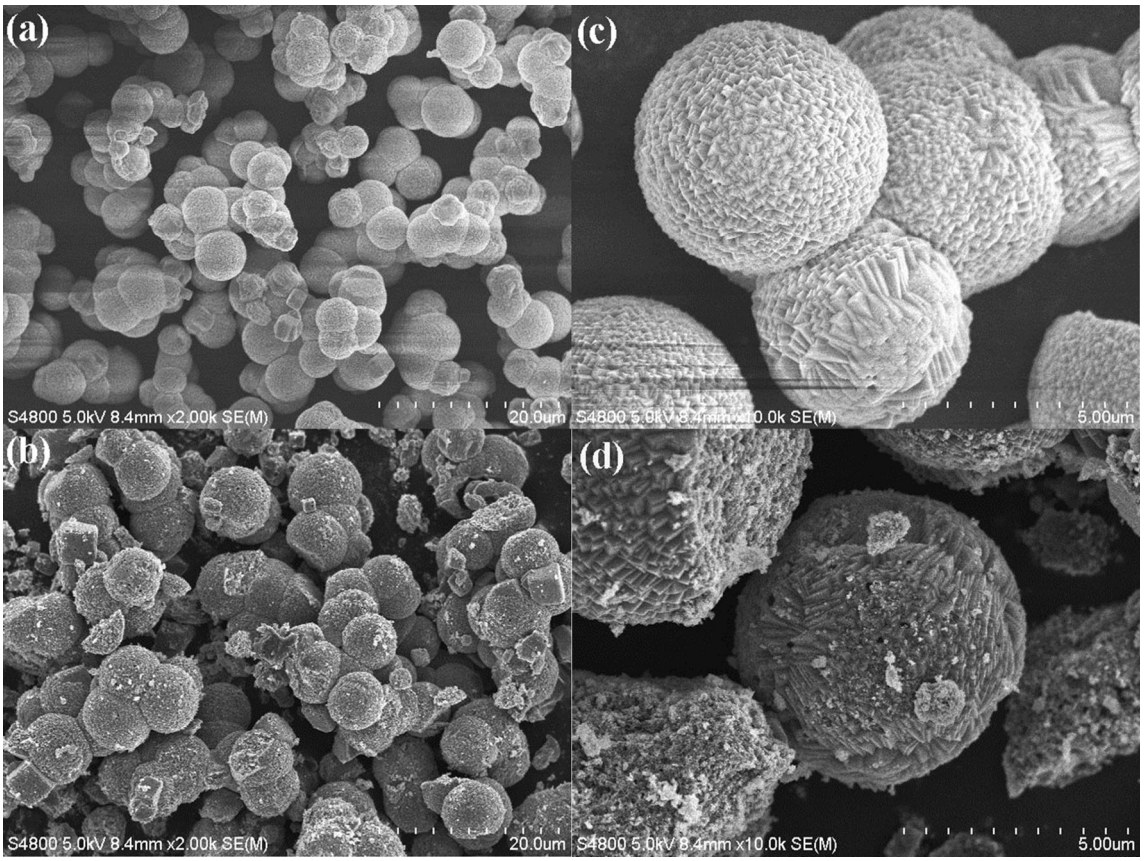

Fig. 2 SEM images of the precursors $MnCO_3$ (**a**, **c**) and Mn_2O_3 (**b**, **d**)

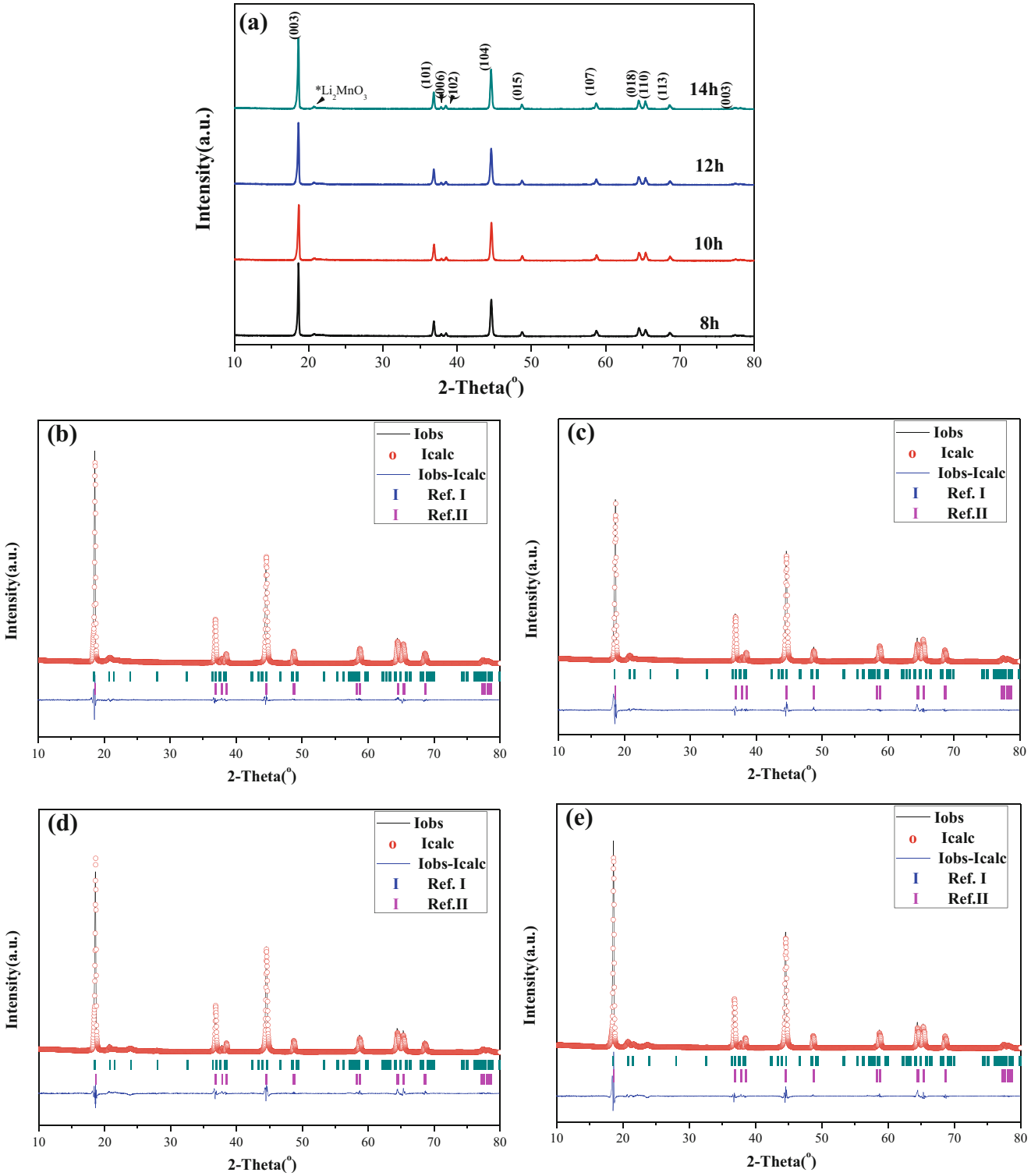

Fig. 3 XRD patterns and Rietveld refinement of cathode material $Li_{1.2}Mn_{0.54}Ni_{0.13}Co_{0.13}O_2$ synthesized at 900° C for different time

a simple solid-state reaction. As the distance for atomic migration is shortened significantly to several nanometers, the undesired particle growth during the annealing is effectively suppressed in the present synthesis. The resultant $Li_{1.2}Mn_{0.54}Ni_{0.13}Co_{0.13}O_2$ exhibit a reasonable discharge capacity and fairly good cycling stability.

Experiments and characterization

Preparation of $MnCO_3$ and MnO_2 microspheres

The $MnCO_3$ microspheres were prepared by a precipitation method. 7.5 mmol of $MnSO_4 \cdot H_2O$ (A.R., Guangdong Guanghua Sci-Tech Co., Ltd.), and 75 mmol of NH_4HCO_3 (A.R., Guangdong Guanghua Sci-Tech Co., Ltd.) was separately dissolved in 500 mL of distilled water. Fifty milliliters of ethanol and the NH_4HCO_3 solution was then added to the $MnSO_4 \cdot H_2O$ solution in sequence under stirring. The mixture was kept under stirring for 1 h at room temperature, then centrifuged, and washed with water for several times. The as-obtained $MnCO_3$ microspheres were dried at 80 °C. The Mn_2O_3 microspheres were synthesized by thermal decomposition of the $MnCO_3$ microspheres at 400 °C for 5 h at air atmosphere.

Preparation of $Li_{1.2}Mn_{0.54}Ni_{0.13}Co_{0.13}O_2$

To obtain $Li_{1.2}Mn_{0.54}Ni_{0.13}Co_{0.13}O_2$ microspheres, stoichiometric amounts of Mn_2O_3 microspheres, $Ni(NO_3)_2 \cdot 6H_2O$ (A.R., Guangdong Guanghua Sci-Tech Co., Ltd.), $LiOH \cdot H_2O$ (A.R., Guangdong Guanghua Sci-Tech Co., Ltd.), and $Co(NO_3)_2 \cdot 6H_2O$ (A.R., Guangdong Guanghua Sci-Tech Co., Ltd.) were mixed and ball-milled for 4 h at a speed of 300 rpm. The $Li_{1.2}Mn_{0.54}Ni_{0.13}Co_{0.13}O_2$ sample was formed by heating the milled precursors at 900 °C for different times in air atmosphere in a muffle furnace.

Material characterization

The crystal structures of the $Li_{1.2}Mn_{0.54}Ni_{0.13}Co_{0.13}O_2$ samples were characterized employing an X-ray diffractometer (Rigaku RINT2000) with Cu Ka radiation and recorded between 10 and 80° with a scanning speed of 3° min^{-1}. The morphologies of the precursors and as-prepared materials were observed using scanning electron microscope (SEM) (Hitachi S4700). Transmission electron microscopy studies of the samples were conducted using a JEM-2100F transmission electron microscope operated at 200 kV.

The electrochemical tests were performed with CR2032 coin-type cells. To fabricate the cathodes, 80 wt% active material, 10 wt% Super P, and 10 wt% polyvinylidene difluoride (PVDF) binder in *N*-methylpyrrolidone (NMP) solution were mixed homogeneously. The resulting slurry was coated on aluminum foil, dried at 120 °C, and pressed with 10 MPa. The resulting cathodes had an active material loading of about 2.5~2.7 mg cm^{-2}. The cells were assembled in an argon-filled box with the moisture content and oxygen levels less than 5 ppm. A metallic lithium foil served as counter and reference electrodes. The electrolyte was 1 M $LiPF_6$ in a mixture of ethylene carbonate and dimethyl carbonate (1:1 in volume). Galvanostatic charge and discharge tests were performed between 2.0 and 4.8 V at room temperature on a battery test system (Neware BTS-5V5mA, China). Cyclic voltammetry tests were carried out at a scanning rate of 0.1 mV s^{-1} between 2.0 and 4.8 V on an electrochemical workstation (ChenHua CHI1040B, China). The electrochemical impedance spectroscopy (EIS) analysis of the fresh cell with the open circuit voltage of the cell about 3.0 V was carried out by applying an AC voltage of 5 mV over the frequency range from 100 kHz to 10 MHz on an electrochemical workstation (Gamery PC14-750, USA). All electrical measurements have been performed at room temperature.

Results and discussion

Figure 1 shows the XRD patterns of the synthesized microsphere $MnCO_3$ and Mn_2O_3 precursor. As shown in Fig. 1a, the diffraction peaks of the precursor $MnCO_3$ are matched well with $MnCO_3$ (JCPDF No. 44-1472) and no impurity is detect-

Table 1 Lattice parameters from the Rietveld refinement of $Li_{1.2}Mn_{0.53}Ni_{0.13}Co_{0.13}O_2$ synthesized at 900° C for different time

Samples		Lattice parameters				Reliability and weighted factors		
		a(A)	b(A)	c(A)	c/a	χ^2	ωRp (%)	Rp (%)
8 h	LMO	4.985706	8.478196	5.11453	1.0258	2.198	0.1051	0.0927
	LNCMO	2.844734	2.844734	14.187813	4.9874			
10 h	LMO	4.989484	8.501032	5.119373	1.0260	2.356	0.1092	0.1101
	LNCMO	2.849943	2.849943	14.216583	4.9884			
12 h	LMO	4.992303	8.51066	5.127297	1.0270	2.232	0.1062	0.1017
	LNCMO	2.852571	2.852571	14.234689	4.9901			
14 h	LMO	4.984111	8.505614	5.115107	1.0263	2.951	0.1178	0.1317
	LNCMO	2.851282	2.851282	14.223689	4.9885			

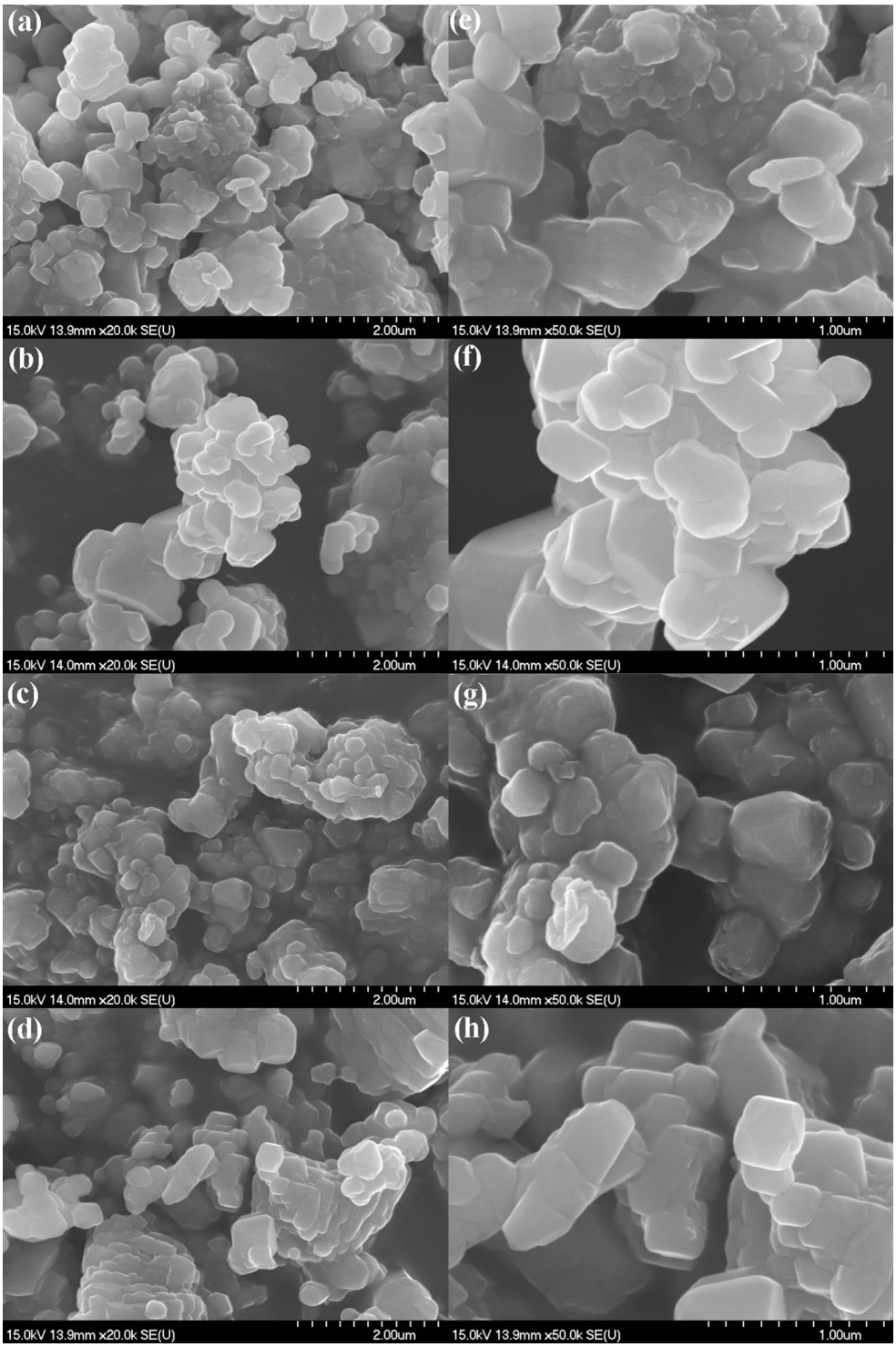

Fig. 4 SEM images of cathode material $Li_{1.2}Mn_{0.54}Ni_{0.13}Co_{0.13}O_2$ synthesized at 900° C for different time: 8 h (**a**, **e**), 10 h (**b**, **f**), 12 h (**c**, **g**), and 14 h (**d**, **h**)

ed, which indicates the $MnCO_3$ microspheres were prepared by a precipitation method. As shown in Fig. 1b, the diffraction peaks of the precursor Mn_2O_3 are matched well with Mn_2O_3 (JCPDF No. 71-0636), which indicates that the Mn_2O_3 microspheres were synthesized by thermal decomposition of the $MnCO_3$ microsphere at 400 °C for 5 h. Thus, the $MnCO_3$ microspheres are converted into Mn_2O_3 by thermal decomposition at 400 °C according to $4MnCO_3+O_2 \rightarrow 2Mn_2O_3+$

$4CO_2$. Besides, Fig. 1b shows that a little impurity phases are indexed as Mn_3O_4 (JCPDF No. 75-0765), which responds with the side reaction $6MnCO_3+3O_2 \rightarrow 3Mn_3O_4+6CO_2$.

In Fig. 2, the SEM images illustrate the morphology of the precursor $MnCO_3$ and Mn_2O_3. As shown in Fig. 2a, c, the precursors $MnCO_3$ exhibited spherical morphology with the size of about 3–6 μm. It is clearly observed from Fig. 2c that the spherical $MnCO_3$ particles have a rough surface and are composed of well-crystalized nanoparticles. Figure 2b, d show that precursor Mn_2O_3 obtained by thermal decomposition of spherical $MnCO_3$ particles retains the microsphere structure with the size of about 6–7 μm. Thus, the use of the pre-grown $MnCO_3$ as the precursor allows for the shape control of the resultant $Li_{1.2}Mn_{0.54}Ni_{0.13}Co_{0.13}O_2$.

Figure 3 shows the diffraction peaks of $Li_{1.2}Mn_{0.54}Ni_{0.13}Co_{0.13}O_2$ synthesized at 900 °C for various times. All the diffraction peaks are indexed by two-phase system consisting of rhombohedral $LiMO_2$ (R-3m, a-$NaFeO_2$ structure) and layered monoclinic Li_2MnO_3 (C2/m). The results were in good agreement with the previous reports [27]. The reflection peaks between 20° and 25° originated from the ordering of lithium ions with transition metal ions in the transition metal layers, corresponding to Li_2MnO_3 phase. Both the (006)/(102) and (108)/(110) doublets are clearly separated, indicating that the well-crystallized layered structures have been formed.

The XRD patterns have been refined by the Rietveld method with General Structure Analysis Software (GSAS Los Alamos National Laboratory, USA) using the approach outlined in Ref. [28]. The refined lattice parameters are listed in Table 1. Because the crystallographic sites of $Li_{1.2}Mn_{0.54}Ni_{0.13}Co_{0.13}O_2$ are shared by more than two cations, it is hard to obtain reliable results on atomic occupancies

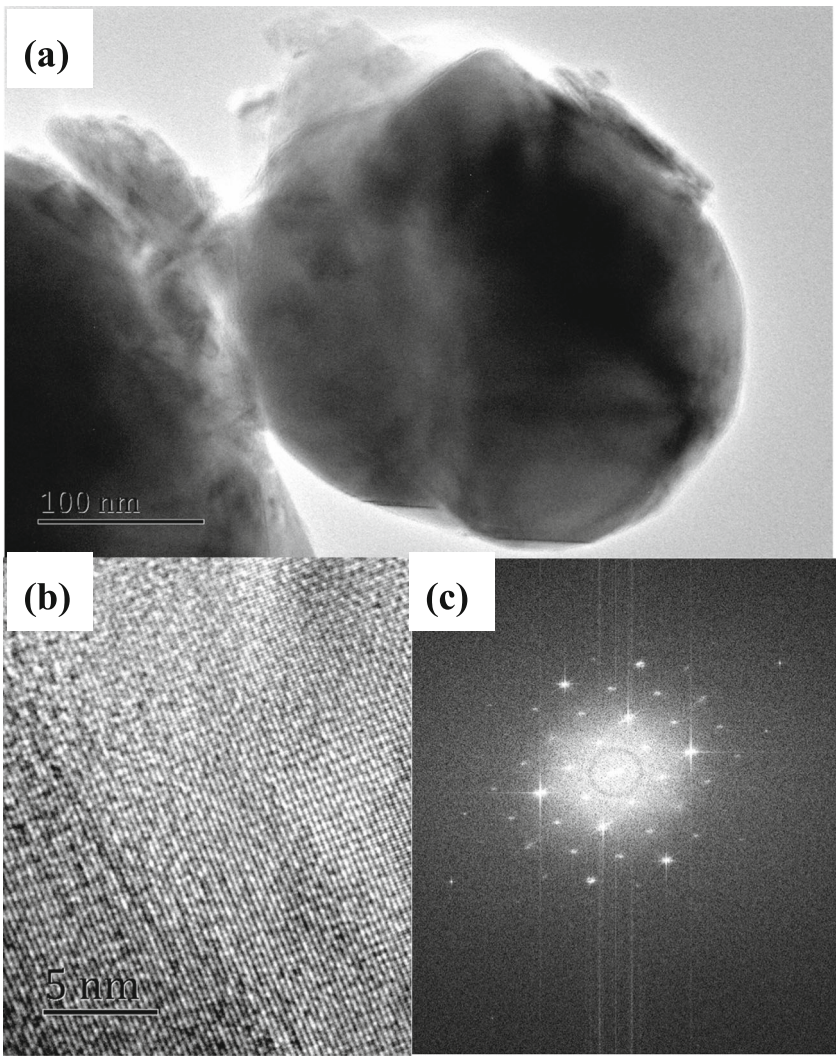

Fig. 5 TEM (**a**), HRTEM (**b**), and Fourier transform (**c**) images of cathode material $Li_{1.2}Mn_{0.54}Ni_{0.13}Co_{0.13}O_2$ synthesized at 900° C for 12 h

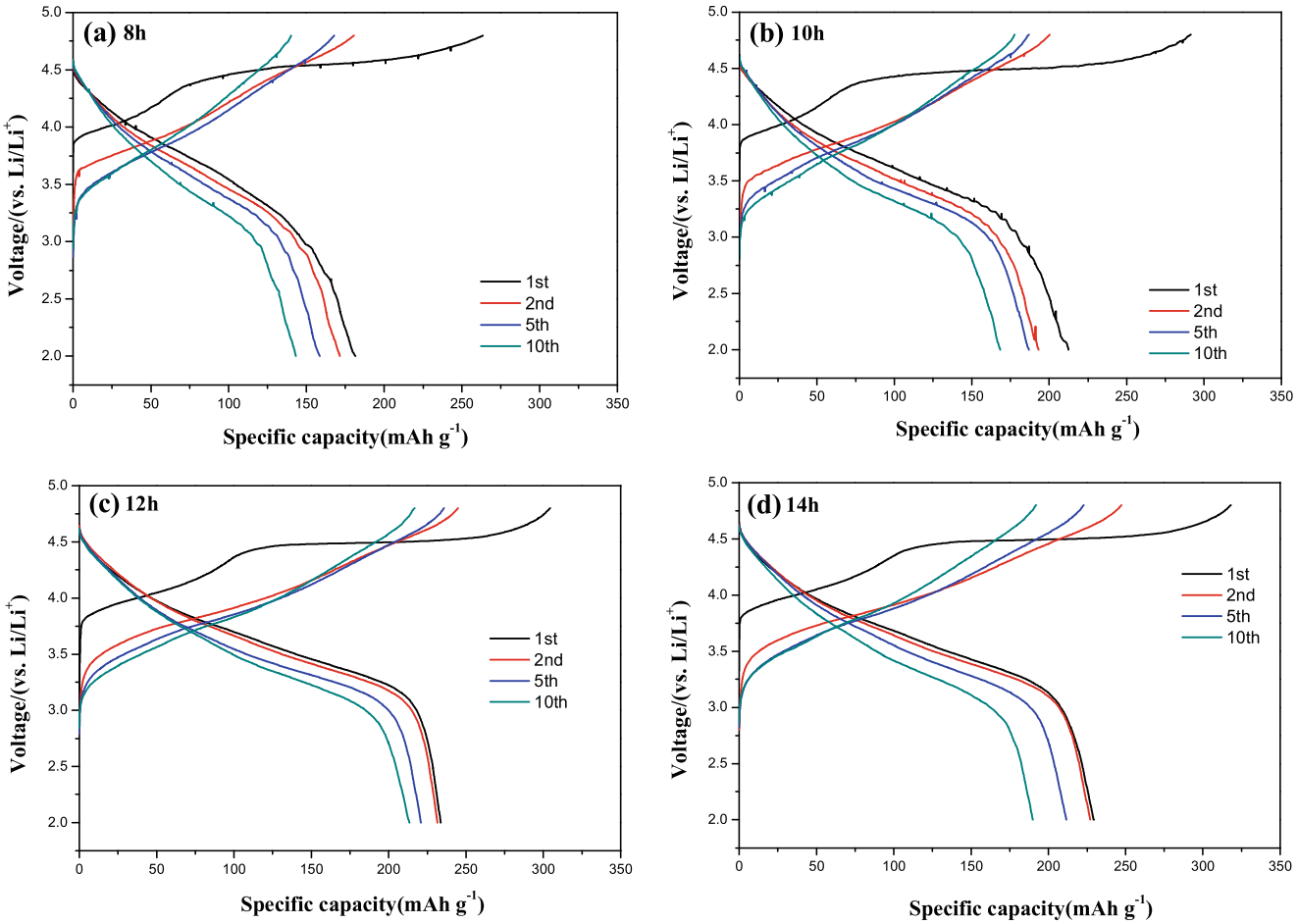

Fig. 6 The charge/discharge curves of cathode material $Li_{1.2}Mn_{0.54}Ni_{0.13}Co_{0.13}O_2$ synthesized at 900° C for different time. The charge rate for fixed at a current of 0.1 C

from the Rietveld refinement. As shown in Ref. [28], the XRD diffraction patterns are refined by the sets of diffraction data: a$NaFeO_2$ type with R-3m and monoclinic Li_2MnO_3 type with C2/m. As listed in Table 1, the cell parameters firstly increase from t=8 h and then reach the maximum till t=12 h and finally decrease with the increasing of calcination time. The increasing lattice parameters can enhance lithium-ion migration in the crystal lattice, which improve its electrochemical performances. These results indicate that the sample synthesized at 900 °C for 12 h has a better electrochemical properties.

In Fig. 4, the SEM images illustrate the morphology of cathode material $Li_{1.2}Mn_{0.54}Ni_{0.13}Co_{0.13}O_2$. As shown in Fig. 4, the as-prepared $Li_{1.2}Mn_{0.54}Ni_{0.13}Co_{0.13}O_2$ is composed of well-crystallized particles with size range from 200 to 500 nm. These nanoparticles have irregular shape. As the calcining time increases, the particles grow up and aggregate more seriously. In order to investigate the detailed morphology, transmission electron microscopy studies on the material synthesized at 900 °C for 12 h are shown in Fig. 5. As shown in Fig. 5a, the micrograph shows that the primary particle of $Li_{1.2}Mn_{0.54}Ni_{0.13}Co_{0.13}O_2$ has regular sphere morphology with a diameter of 320 nm. The Fig. 5b shows that the particles are high crystalline, and the lattice fringes are found to be about 0.204 nm, corresponding to the d104 and d202 spacing in the XRD patterns of rhombohedral $LiMO_2$ (R-3m) and layered monoclinic Li_2MnO_3 (C2/m), respectively. Furthermore, as shown in the Fig. 5c, the Fourier transform images exhibit spot patterns suggesting highly crystalline structures, which are in accordance with XRD results.

Figure 6 exhibits the charge-discharge curves of the $Li_{1.2}Mn_{0.54}Ni_{0.13}Co_{0.13}O_2$ synthesized at 900 °C for various times operated at 0.1 C (1 C=180 mA g^{-1}). Similar charge-discharge profiles can be observed in Fig. 6. All the initial charge curves clearly displayed two plateaus located at 3.7–4.5 V and above 4.5 V. The first plateau is ascribed to lithium ion extraction from the layered $LiCoO_2$ and $LiNiO_2$ structure [28]. The second plateau could be attributed to the oxygen loss process from the Li_2MnO_3 component, which results in high irreversible capacity of $Li_{1.2}Mn_{0.54}Ni_{0.13}Co_{0.13}O_2$ electrode [28]. The initial discharge capacities are 181.4, 213.5, 233.6,

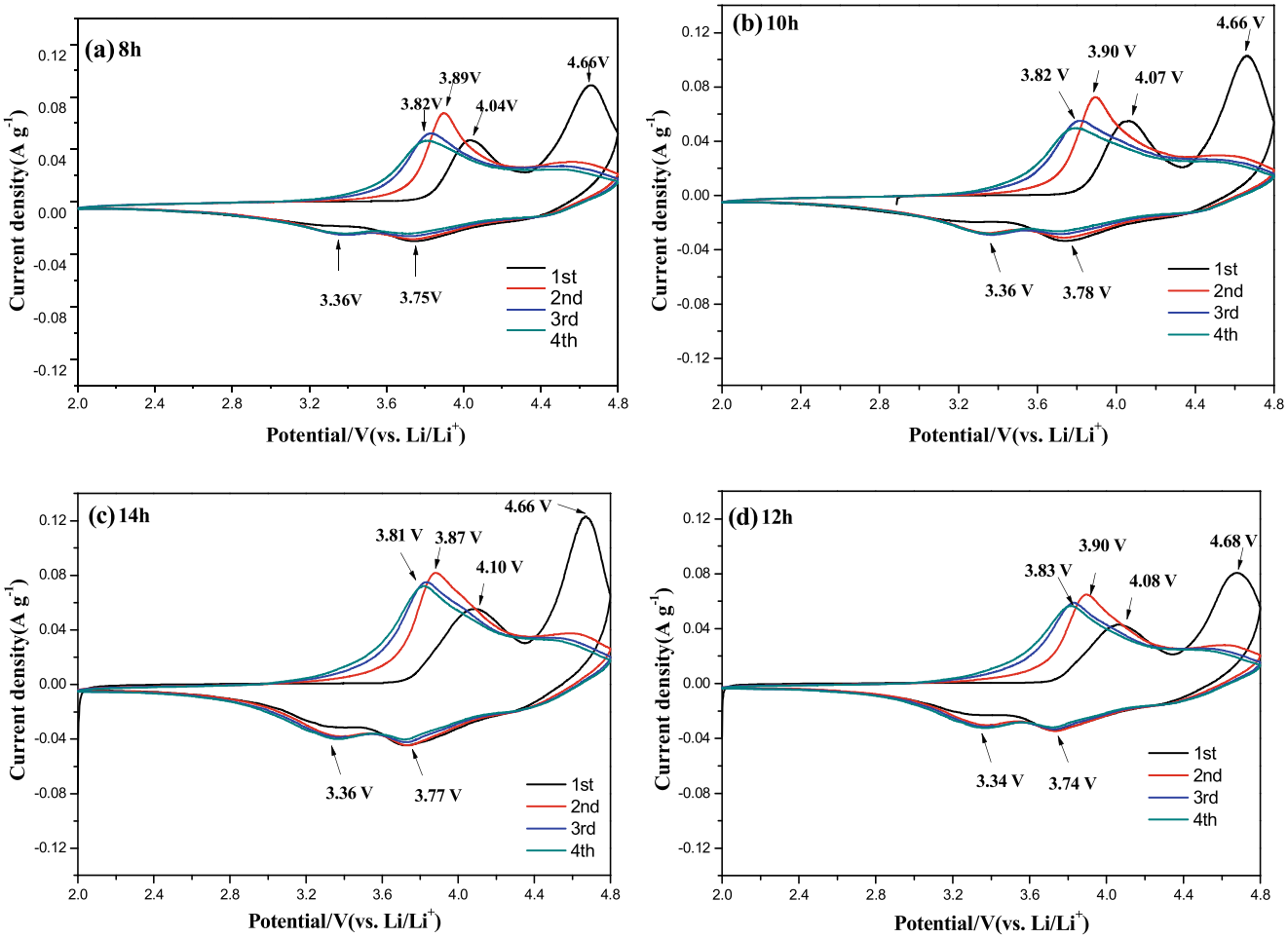

Fig. 7 Cyclic voltammetry curves of cathode material $Li_{1.2}Mn_{0.54}Ni_{0.13}Co_{0.13}O_2$ synthesized at 900° C for different time

and 229.4 mAh g^{-1} for 8, 10, 12, and 14 h, respectively. After 10 cycles, the discharge capacities retain 143.3, 167.4, 214.3, 189.8 mAh g^{-1}, respectively. The capacity retentions are 78.4, 79.2, 91.7, and 82.7 %, respectively. The results indicate the sample synthesized at 900 °C for 12 h has the best electrochemical performances.

To further investigate the electrochemical behaviors of the $Li_{1.2}Mn_{0.54}Ni_{0.13}Co_{0.13}O_2$ synthesized at 900 °C for various time, cyclic voltammetry (CV) was conducted on the electrode at the scan rate of 0.1 mV s^{-1} between 2.0 and 4.8 V and the results are shown in Fig. 7. The two oxidation peaks at 4.06 and 4.75 V in the first cycle corresponded to the

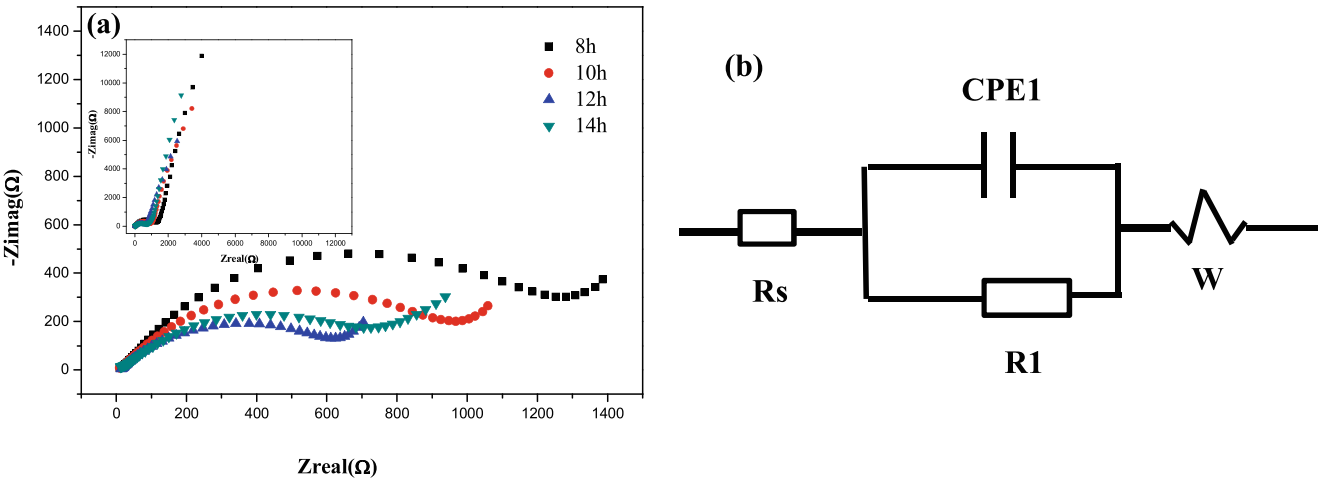

Fig. 8 Nyquist plots (**a**) and the equivalent electric circuit (**b**) of cathode material $Li_{1.2}Mn_{0.54}Ni_{0.13}Co_{0.13}O_2$ synthesized at 900° C for different time

Table 2 Impedance parameters derived from the equivalent circuit for the cathode material $Li_{1.2}Mn_{0.53}Ni_{0.13}Co_{0.13}O_2$ synthesized at 900° C for different time

Sample	Rs (Ω)	CPE-T (10^{-5} S cm^{-2})	CPE-P (S cm^{-2})	Rct (Ω)	Chi-square
8 h	23.64	1.920	0.74646	1446	0.00036435
10 h	17.99	2.33190	0.69349	1067	0.00010558
12 h	12.66	4.20390	0.63091	705.2	0.00021517
14 h	20.86	2.67090	0.63723	833.2	0.00082771

oxidation of the Ni^{2+} and Co^{3+} ions and the release of oxygen, respectively. The reduction peaks at 4.45 and 3.79 V in the first cycle could be ascribed to the reduction of Ni^{4+} and Co^{4+} ions. In the second and third cycles, the CV profiles are significantly different from that observed in the first cycle. A new weak oxidation peak emerges at 4.6 V with the disappearance of the strong oxidation peak at 4.7 V. The two oxidation peaks at 3.9 and 4.6 V could be attributed to the oxidation of Ni^{2+} and Co^{3+}, respectively. The negative shift of Mn^{4+}/Mn^{3+} reduction peak with cycles evidenced the structure transformation from layered to a layered-spinel intergrowth structure [29].

Furthermore, electrochemical impedance spectroscopy (EIS) is used to analyze the electrochemical properties of $Li_{1.2}Mn_{0.54}Ni_{0.13}Co_{0.13}O_2$ synthesized at 900 °C for various time. As shown in Fig. 8a, the Nyquist plots of the cells consist of barely visible semicircles alike in appearance of a half ellipse (in the high frequency ranges) and a straight line with changing slope to the real axes (in the lower frequency range). The study of the EIS results has been performed by using the approach outlined in Ref. [19, 30, 31] by using an equivalent circuit model shown in Fig. 8b. The fitting results derived from the equivalent circuit are presented in Table 2. Generally, an intercept at the Zreal axis at a high frequency corresponds to the ohmic resistance (Rs), which represents the total resistance of the electrolyte, separator, and electrical contacts. The depressed semicircle in the high frequency range indicates the charge transfer resistance (Rct). The inclined line in the lower frequency range represents the Warburg impedance and corresponds to the lithium diffusion kinetics towards the electrodes. As shown in Table 2, the electrolyte resistance remained almost constant, which was expected since the variation of an electrolyte concentration was not so large as to affect the electrolyte conductivity. The transfer resistance (Rct) of the sample synthesized at 12 h is smaller than the other ones, indicating that the $Li_{1.2}Mn_{0.54}Ni_{0.13}Co_{0.13}O_2$ synthesized at 900 °C 12 h has better electrochemical performances. These results are in accordance with above results.

The initial charge-discharge curve and cyclic performance of the sample prepared at 900 °C for 12 h at the rate of 0.1, 0.2, 0.5, and 1 C for 50 cycles are presented in Fig. 9a, b, respectively. As shown in Fig. 9a, the sample has the similar shape and delivers discharge capacities of 233.5, 214.2, 199.3, and 168.1 mAh g^{-1} at 0.1, 0.2, 0.5, and 1 C, respectively. After 50 cycles, the capacity retains 178.0, 166.3, 162.1, and 155.9 mAh g^{-1} at 0.1, 0.2, 0.5, and 1 C, respectively. The capacity retentions are 76.2, 77.6, 81.3, and 92.7 %, respectively. These results indicate that the simple and feasible morphology and size control synthesis has a great potential in manganese-based electrode materials. However, the high initial irreversible capacity and poor cycle performances especially in high rate still can be observed. It should be ascribed to the irreversible the oxygen loss process and the side reactions of the cathode surface with electrolyte [32, 33]. Further works,

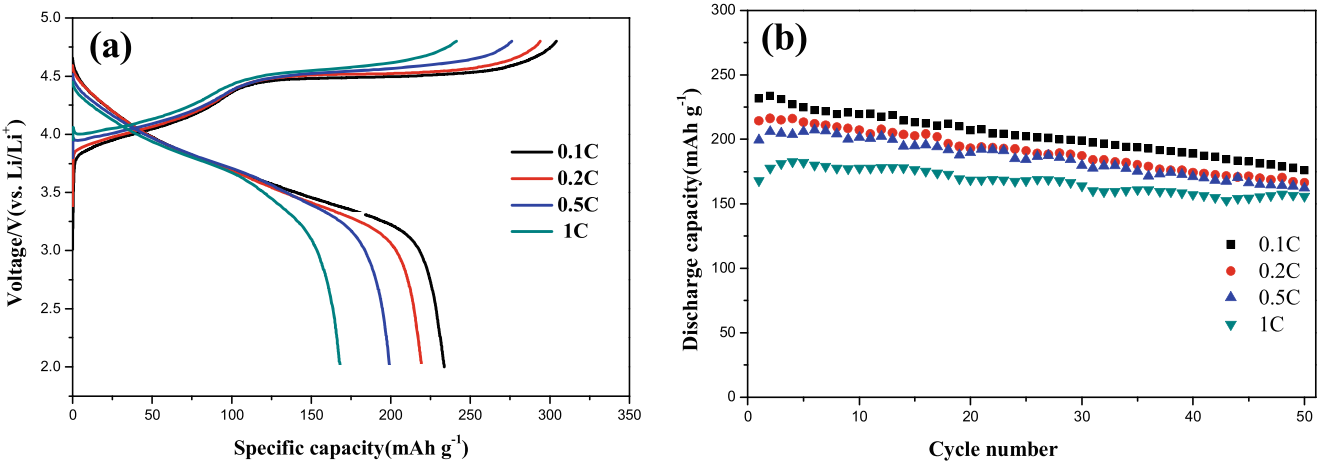

Fig. 9 The initial charge/discharge curves and cycle performances of cathode material $Li_{1.2}Mn_{0.54}Ni_{0.13}Co_{0.13}O_2$ synthesized at 900° C for 12 h

such as doping, surface coating, and electrolyte additive, are necessary to improve the electrochemical performance.

Conclusions

$Li_{1.2}Mn_{0.54}Ni_{0.13}Co_{0.13}O_2$ microspheres have been successfully synthesized by the morphology-controlled solid-state method. XRD, SEM results show well-crystallized $Li_{1.2}Mn_{0.54}Ni_{0.13}Co_{0.13}O_2$ microspheres have been obtained. Electrochemical tests show the as-prepared material synthesized at 900 °C for 12 h displays better electrochemical performances. The initial discharge capacities are 233.5, 214.2, 199.3, and 168.1 mAh g^{-1} at 0.1, 0.2, 0.5, and 1 C, respectively. After 50 cycles, the capacity retains 178.0, 166.3, 162.1, and 155.9 mAh g^{-1} at 0.1, 0.2, 0.5, and 1 C, respectively. In summary, the results demonstrated that the state-of-art $Li_{1.2}Mn_{0.54}Ni_{0.13}Co_{0.13}O_2$ can be synthesized with the unique solid-state method. The simple method could pave the road for the scale-up production of the advanced manganese-based cathode materials for Li-ion batteries.

Acknowledgments This work is supported by the project of Innovative group for high-performance lithium-ion power batteries R&D and industrialization of Guangdong Province (Grant No. 2013N079), State Key Laboratory of Chemical Engineering (No. SKL-ChE-14B0 4), Shenzhen Peacock Plan Program (KQCX20140521144358003), and Fundamental Research Plan of Shenzhen (JCYJ20140417172417144).

References

1. Tarascon JM, Armand M (2001) Nature 414:359–367
2. Bruce PG, Scrosati B, Tarascon JM (2008) Angew Chem Int Ed 47: 2930–2946
3. Chen J, Cheng FY (2009) Acc Chem Res 42:713–723
4. Padhi AK, Nanjundaswamy KS, Goodenough JB (1997) J Electrochem Soc 144:1189–1194
5. Lee HW, Muralidharan P, Ruffo R, Mari CM, Cui Y, Kim DK (2010) Nano Lett 10:3852–3856
6. Lee ES, Huq A, Chang HY, Manthiram A (2012) Chem Mater 24: 600–612
7. Wu F, Tian J, Su YF, Guan YB, Jin Y, Wang Z, He T, Bao LY, Chen S (2014) J Power Sources 269:747–754
8. Kang SF, Qin HF, Fang Y, Li X, Wang YG (2014) Electrochim Acta 144:22–30
9. Wu F, Wang Z, Su YF, Yan N, Bao LY, Chen S (2014) J Power Sources 247:20–25
10. He F, Wang XQ, Du CQ, Baker AP, Wu JW, Zhang XH (2015) Electrochim Acta 153:484–491
11. Jiang X, Wang ZH, Rooney D, Zhang XX, Feng J, Qiao JS, Sun W, Sun KN (2015) Electrochim Acta 160:131–138
12. Zhu Y, Zhu LW (2014) J Power Sources 256:178–182
13. Yang SY, Huang G, Hua SJ, Hou XH, Huang YY, Yue M, Lei GT (2014) Mater Lett 118:8–11
14. Ju JH, Cho SW, Hwang SG, Yun SR, Lee Y, Jeong HM, Hwang MJ, Kim KM, Ryu KS (2011) Electrochim Acta 56:8791–8796
15. Liu XY, Liu JL, Huang T, Yu AS (2013) Electrochim Acta 109:52–58
16. Shi SJ, Tu JP, Tang YY, Liu XY, Zhang YQ, Wang XL, Gu CD (2013) Electrochim Acta 88:671–679
17. Song BH, Lai MO, Lu L (2012) J Power Sources 80:187–195
18. Singh G, Thomas R, Kumar A, Katiyar RS (2012) J Electrochem Soc 159:410–420
19. Yang M, Du CQ, Tang ZY, Wu JW, Zhang XH (2014) Ionics 20: 1039–1046
20. Sun ST, Du CQ, Wu JW, Tang ZY, Yang M, Zhang XH (2014) Ionics 20:1627–1634
21. Zhan D, Yang F, Zhang QG, Hu XH, Peng TY (2014) Electrochim Acta 129:364–372
22. Zhu Z, Yan H, Zhang D, Li W, Lu Q (2013) J Power Sources 224: 13–19
23. Wang JW, Liu J, Yang GL, Zhang XF, Yan XD, Pan XM, Wang RS (2009) Electrochim Acta 54:6451–6454
24. Yang JG, Cheng FY, Zhang XL, Gao HY, Tao ZL, Chen J (2014) J Mater Chem A 2:1636–1640
25. Shaju KM, Bruce PG (2008) Dalton Trans, 5471–5475
26. Dai KH, Mao J, Li ZT, Zhai YC, Wang ZH, Song XY, Battaglia V, Liu G (2014) J Power Sources 248:22–27
27. Shi SJ, Lou ZR, Xia TF, Wang XL, Gu CD, Tu JP (2014) J Power Sources 257:198–204
28. Miao XW, Ni H, Zhang H, Wang CG, Fang JH, Yang G (2014) J Power Sources 264:147–154
29. Johnson CS, Li N, Lefief C, Vaughey JT, Thackeray MM (2008) Chem Mater 20:6095–6106
30. Jang IC, Son CG, Yang SMG, Lee JW, Cho AR, Aravindan V, Park GJ, Kang KS, Kim WS, Cho WI, Lee YS (2011) J Mater Chem 21: 6510
31. Du CQ, Wu JW, Liu J, Yang M, Xu Q, Tang ZY, Zhang XH (2015) Electrochim Acta 152:473–479
32. Li GR, Feng X, Ding Y, Ye SH, Gao XP (2012) Electrochim Acta 78:308–315
33. Fu Q, Du F, Bian XF, Wang YH, Yan X, Zhang YQ, Zhu K, Chen G, Wang CZ, Wei YJ (2014) J Mater Chem A 2:7555–7562